



TECHNICAL ARTICLE

Morphology and Corrosion Resistance of Hydroxyapatite Coatings Formed on Commercially Pure Titanium

O.V. Tkachuk, I.M. Pohrelyuk, R.V. Proskurnyak, J. Morgiel, M. Faryna, and A. Goral

Submitted: 12 January 2022 / Revised: 31 December 2022 / Accepted: 13 January 2023 / Published online: 9 February 2023

The porous hydroxyapatite coatings with a spherical structure were formed on commercially pure titanium (CP-Ti) by the micro-arc oxidation (MAO) in an alkaline electrolyte (hydroxyapatite + 1 M potassium hydroxide) at the applied voltage of 140, 160, 180 V and deposition time of 1 and 2 min. It was determined that by increasing voltage from 140 to 160 V the Ca/P ratio increases from 1.54 to 1.69, i.e., the composition of hydroxyapatite (HA) approaches to the biological one that accelerates formation of the interfacial bond between the implant and bone tissue. It was shown that increasing deposition time from 1 to 2 min at the voltage of 140 V promotes increasing Ca/P ratio. The corrosion resistance of CP-Ti with HA coatings was studied in Ringer's solution at a temperature of 37 °C. The best corrosion protection was observed for the coating deposited at 160 V, 1 min, when the thickness of the coating and HA formation is the highest.

Keywords corrosion resistance, CP-Ti, hydroxyapatite coatings, micro-arc oxidation, Ringer's solution

1. Introduction

Hydroxyapatite [Ca₁₀(PO₄)₆(OH)₂; HA] is widely used to enhance the osseointegration of titanium implants. Micro-arc oxidation (MAO) is one of the methods for formation of such bioceramic coating that increases not only the biocompatibility of titanium, but also its wear and corrosion resistance (Ref 1-7). Tuning parameters of the deposition process (deposition time, applied voltage) and the electrolyte composition allow to obtain a required morphology, phase composition and thickness of the MAO coating (Ref 8-14). The electrolyte is selected by the ability of its components to form hydroxyapatite with a ratio of Ca/P = 1.67.

The electrolytes containing calcium acetate and glycerophosphate or β -glycerophosphate are widely used (Ref 15). S. Durdu et al. (Ref 16) formed HA and calcium apatite-based coatings on Ti6Al4V alloy in an electrolyte containing calcium acetate and β -calcium glycerophosphate for 1...120 min. The coating surface had a porous structure, and the highest amount of crystalline HA was observed for coating formed at 120 min. It was shown the efficiency of formation of calcium-phosphate coatings on the surface of Ti₆Al₄V alloy during the MAO adding hydroxyapatite powder to the electrolyte containing 0.12 M Na₃PO₄ (NAP) (Ref 17). It was found that the content of hydroxyapatite and tricalcium

phosphate, as well as the thickness and roughness of the coating surface, increase as the concentration of HA rises from 1 to 2 g/l.

Shokouhfar et al. (Ref 18, 19) investigated the effect of KOH on the formation of oxide coatings on titanium by MAO under constant pulsed DC current. It was shown that the addition of KOH to the electrolyte provides high surface homogeneity and better corrosion resistance in Ringer's solution. According to investigations of Okido et al. (Ref 20), increasing pH electrolyte by adding sodium hydroxide (NaOH) promotes the increasing content of hydroxyapatite phase. The influence of the concentration of electrolyte component (NaOH) on the phase composition, microstructure, Ca/P, bond strength and corrosion resistance of MAO coatings on Ti-6Al-4 V alloy was determined (Ref 21). As the NaOH concentration increased from 5 to 15 g/l, the Ca/P coating ratio enhanced from 0.56 to 2.36 and the bond strength from 18.55 to 63.36 MPa. It was also observed unevenly distributed porosity and an improvement of corrosion resistance of the alloy with MAO coatings in 3.5% NaCl. Finally, the addition of NaOH or KOH to the electrolyte allows to increase its pH that will enhance the electrical conductivity and facilitate the formation of hydroxyapatite coating during MAO. Anawati et al. (Ref 22) showed that corrosion resistance of Ti-HA composites containing 0-10% HA in 0.9 NaCl solution at 36.5 °C was higher compared to CP-Ti. Formation of hydroxyapatite phase improves the corrosion resistance of titanium alloys in simulated body fluids as documented by other authors (Ref 23-25).

In our previous work (Ref 26), the calcium phosphate coatings were formed on CP-Ti by MAO in 3% solution of an orthophosphoric acid with the addition of hydroxyapatite powder. MAO coating formed at 220 V provided higher corrosion resistance in Ringer's solution at 37 °C than coatings deposited at 180 and 200 V. However, the Ca/P ratio was 0.5, which is significantly different from Ca/P for biological hydroxyapatite. An increase in the Ca/P ratio could be realized by replacing the acidic electrolyte with the alkaline one. Therefore, the aim of this work is to study the composition, structure and corrosion resistance of hydroxyapatite coatings

O.V. Tkachuk, I.M. Pohrelyuk, and R.V. Proskurnyak, Karpenko Physico-Mechanical Institute of the National Academy of Sciences of Ukraine, 5 Naukova Str., Lviv 79060, Ukraine; **J. Morgiel, M. Faryna, and A. Goral**, Institute of Metallurgy and Materials Science of Polish Academy of Sciences, 25 Reymonta Str., 30-059 Krakow, Poland. Contact e-mail: tkachukoleh@gmail.com.

formed on CP-Ti in the alkaline electrolyte containing 1 M KOH and hydroxyapatite powder.

2. Materials and Methods

The hydroxyapatite coatings were formed on CP-Ti samples ($a = 10$ mm, $b = 5$ mm; $h = 1$ mm) by the MAO where titanium was used as the anode, and a titanium mesh (for better electrolyte circulation) as the cathode. The MAO process was performed at the applied voltage of 140; 160 and 180 V for 1 and 2 min; an initial current density was 0.29 A/cm² (pulse current). The electrolyte composition for MAO was as follows (in g/l): Ca₁₀(PO₄)₆(OH)₂-100; KOH-56.

The phase composition of the deposited layers was determined by x-ray phase analysis on a D8 Bruker Discover diffractometer (focusing according to the Bragg–Brentano scheme, CoK α radiation). The voltage at the anode of the x-ray tube was 40 kV at a current of 45 mA. Surface microstructure of the MAO layers was carried out by scanning electron microscope (SEM) FEI Quanta 3D FEGSEM integrated with the EDAX Trident system. The cross section of the MAO specimens was studied by scanning electron microscope EVO-40XVP with an INCA Energy 350 energy-dispersive x-ray spectrometer.

The corrosion resistance of hydroxyapatite coatings deposited on titanium substrate was tested in Ringer's solution at a temperature of 37 ± 0.5 °C by chronopotentiometry using a potentiostat/galvanostat IPCpro for 30 min, as well as by the method of volt-ampere characteristic with a scan rate of 5 mV/s in the potential range of $-1.0 \dots 2.0$ V versus Ag/AgCl. The surface of the working electrode made of CP-Ti was coated with epoxy resin, leaving 1 cm² area for the exposure to the electrolyte. The electrochemical impedance spectroscopy (EIS) measurements were carried out at OCP with a voltage amplitude of 10 mV and frequency range from 10,000 to 0.01 Hz. The measures were repeated at least three times, and the experimental data were fitted with the software Z-View using proper equivalent circuit. Impedance spectra were reported by the Nyquist diagram.

3. Results and Discussion

According to x-ray phase analysis (Fig. 1), the phases of calcium titanate CaTiO₃ (22-153), dicalcium phosphate anhydrite CaHPO₄ (3-423) and hydroxyapatite Ca₁₀(PO₄)₆(OH)₂ (3-747; 00-064-0738) represented by reflections (020), (121) and (002) were detected on the surface of CP-Ti after MAO at the applied voltage of 140, 160 and 180 V (Fig. 1a, b, c). The reflections of HA phase were intensified with increasing voltage from 140 to 160.

The porous coating prepared by MAO on titanium surface at the applied voltage of 140 V and deposition time of 1 min is built of empty spherical particles, what is characteristic of HA materials (Fig. 2a). Areas carrying markings of surface etching, as well as local thermal cracks, were also noted. In addition to open pores, there are closed small pores formed on the surface at increasing spark discharge energy. The porosity of the MAO coating was 10.7%. The small pores in the range of $0.07 \dots 3$ μ m are predominant (92.3%); the content of pores

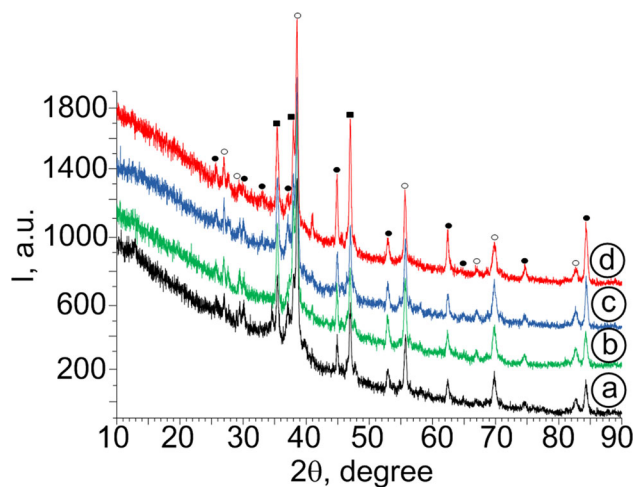


Fig. 1 X-ray diffraction patterns of CP-Ti after MAO for 1 min: 140 V (a), 160 V (b), 180 V (c); 2 min: 140 V (d); ● – HA, ○ – CaTiO₃, ■ – CaHPO₄

with a size of $4 \dots 11$ μ m was 7.7% (Fig. 3a). The average pore size is 3.6 μ m. According to energy-dispersive x-ray (EDS) analysis, the Ca/P ratio is ~ 1.54 .

At a voltage of 160 V (Fig. 2b), a uniform porous coating with a spherical structure is formed. Numerous spherical HA nanocrystals with a size of 80-160 nm are attached to the sample surface. Increasing applied voltage to 160 V leads to decreasing small pores to 90.5% and increasing number of pores in the range of $3.5 \dots 14$ μ m (9.5%) (Fig. 3b). The porosity increases to 11.7%, and the average pore size is 5.45 μ m. According to EDS analysis, the ratio Ca/P = 1.69, which is close to the ratio proper for biological hydroxyapatite (1.67). It should be noted that such microstructure can be useful for the HA film, as it can accelerate the formation of the interfacial bond between the implant and bone tissue (Ref 24).

By rising applied voltage to 180 V (Fig. 2c), the porosity of HA coating increases by 1.4 times, but there is a significant etching of the surface. It reduces the number of small pores in the range of $0.07 \dots 1$ μ m (59.2%), pores with a size of $1.33 \dots 3$ μ m-28.4%, and $3.3 \dots 13$ μ m-12.5% (Fig. 3c). The average pore size is 4.11 μ m. Since, according to the EDS analysis, the Ca/P ratio decreases to 1.57, so the MAO at 180 V is ineffective to form the HA coating.

In addition to the effect of applied voltage, the influence of deposition time of the MAO on the formation of HA coating on CP-Ti was investigated. At the voltage of 140 V by doubling time from 1 to 2 min, the content of HA phase in the coating increases that is confirmed by raising of the intensity of its reflections in the diffraction spectrum (the reflections of CaTiO₃ and CaHPO₄ phases remained fixed) (Fig. 1a, b). According to SEM observations, a uniform porous coating with a spherical structure is formed on titanium surface; microcracks are observed on the surface (Fig. 2d). Simultaneously, a number of HA nanocrystals increases significantly. At longer time, the spherical nanoparticles with a size of 60-120 nm are formed (Fig. 4). Prolonging deposition time increases the content of calcium and phosphorus at the surface layer. The Ca/P ratio increases to 1.64 that is close to the value for biological hydroxyapatite. The porosity of HA coatings deposited for different time is similar. The number of small pores decreases in the range of $0.07 \dots 1$ μ m to 59.4%, pores with a size of

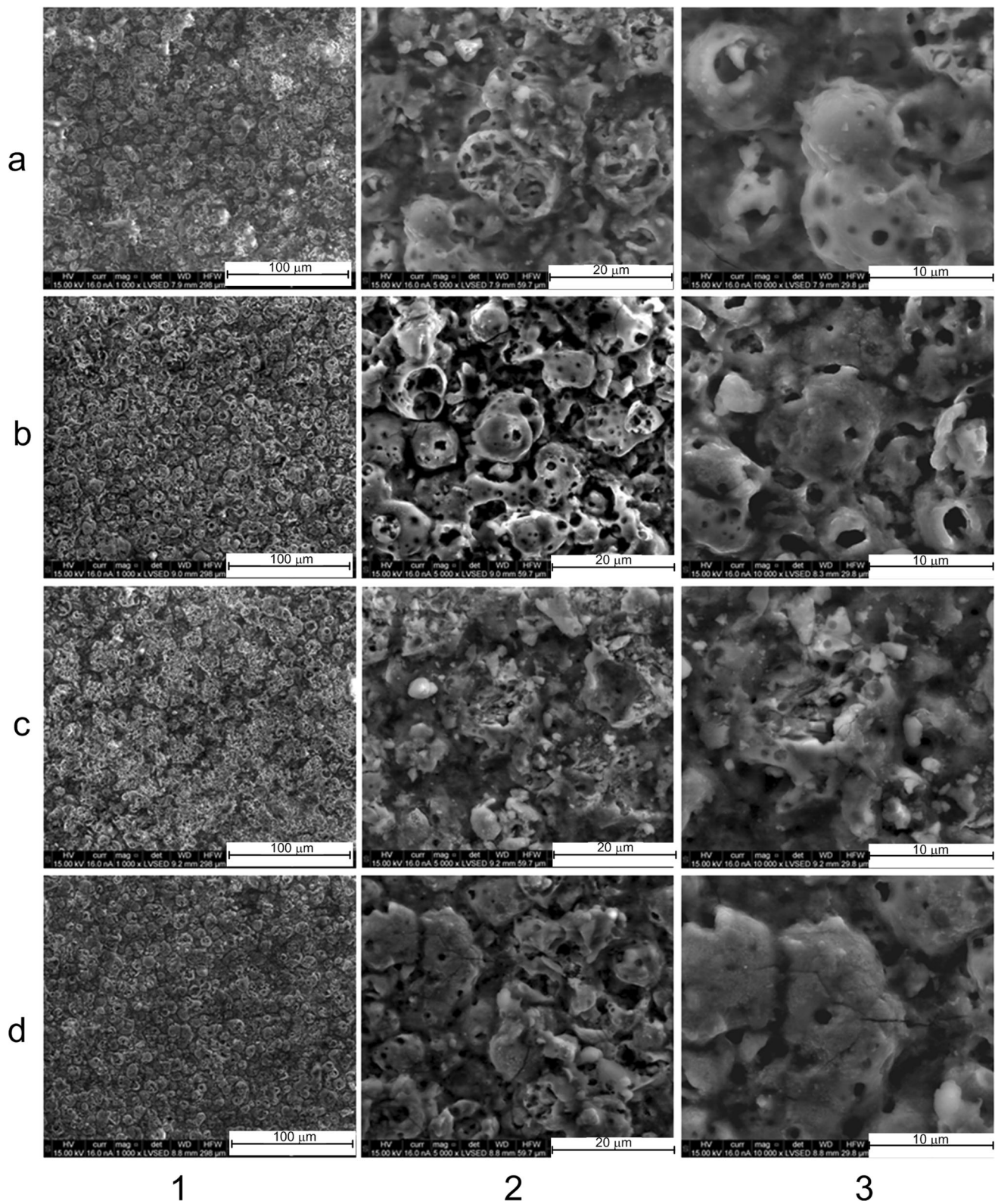


Fig. 2 FEGSEM images of CP-Ti with hydroxyapatite coatings formed after 1 min of MAO: 140 V (a); 160 V (b); 180 V (c); 2 min: 140 V (d); 1 ($\times 1000$), 2 ($\times 5000$) and 3 ($\times 10,000$) magnification images are presented at the left, middle and right columns, respectively

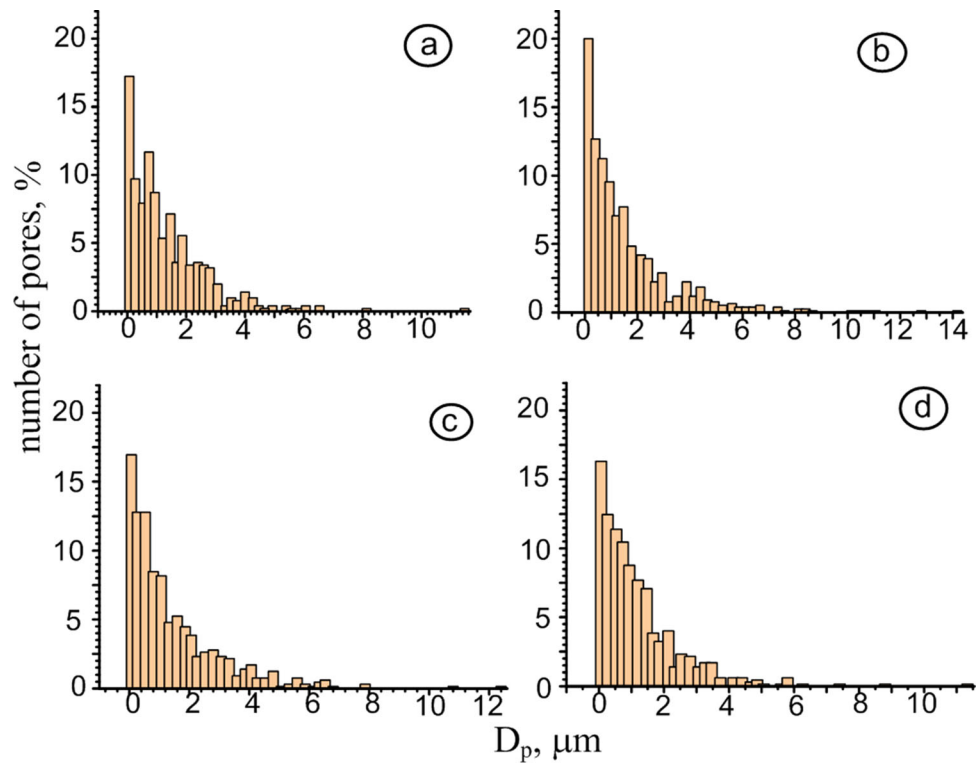


Fig. 3 Histograms of pore size distribution in hydroxyapatite coatings formed on surface of CP-Ti after 1 min of MAO: 140 V (a); 160 V (b); 180 V (c); 2 min: 140 V (d)

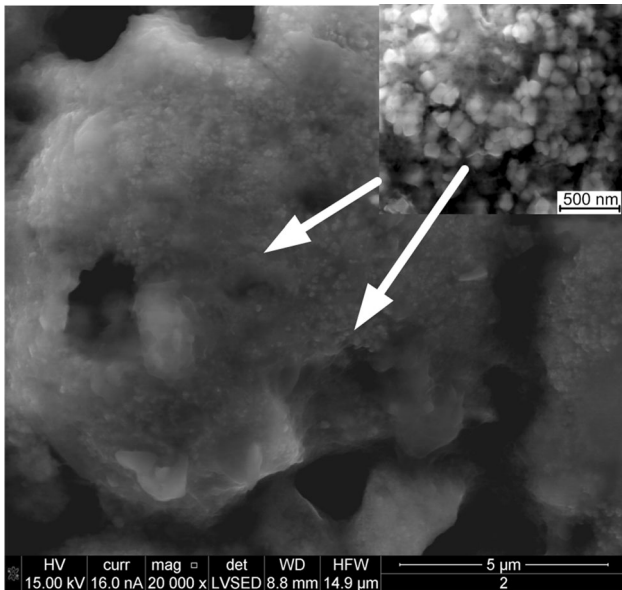


Fig. 4 Surface morphology of MAO coating: 140 V, 2 min; $\times 20,000$ and $\times 150,000$ magnifications

1.2...5 μm -39.23%, 6...12 μm -1.4% (Fig. 3d). The average pore size is 3.59 μm .

The morphology of the cross section of MAO coatings deposited on the surface of CP-Ti at 160 V, 1 min and 140 V, 2 min is shown in Fig. 5 and 6. The top layer is MAO coating, and the bottom layer is titanium substrate. The morphology of MAO coatings in Fig. 5, 6 illustrates that both coatings are compact but differ in thickness (65 and 85 μm). The bonding between the MAO coating and Ti substrate shows no interfacial cracks or voids. The EDS scan was performed along the interfacial region of the cross sections documenting sharp change of composition at the coating/substrate interface.

Figure 5 and 6 also illustrates in depth concentration profiles of calcium, titanium, phosphorus and oxygen. They indicate that the thickness of the HA layer formed at 160 V, 1 min is $\sim 25 \mu\text{m}$, and at 140 V, 2 min-30 μm . A further decrease in the concentration of the previous mentioned elements and an increase in titanium content point toward presence of CaTiO_3 and CaHPO_4 phases as separately documented by the x-ray phase analysis.

Figure 7 presents changes of the open circuit potential (OCP) against time for CP-Ti with HA coatings in Ringer's solution at a temperature of 37 $^\circ\text{C}$. For the HA coating deposited at the applied voltage of 140 V (Fig. 7, curve 1), the

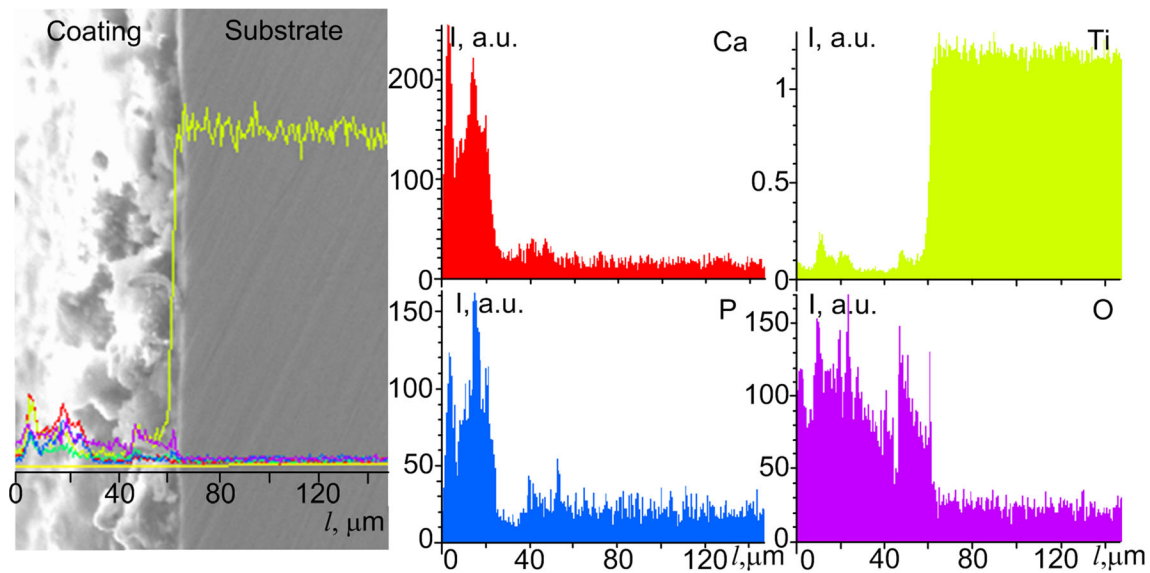


Fig. 5 SEM cross-sectional image of the MAO specimen prepared at 160 V for 1 min, and EDS depth profiles of calcium, titanium, phosphorus and oxygen

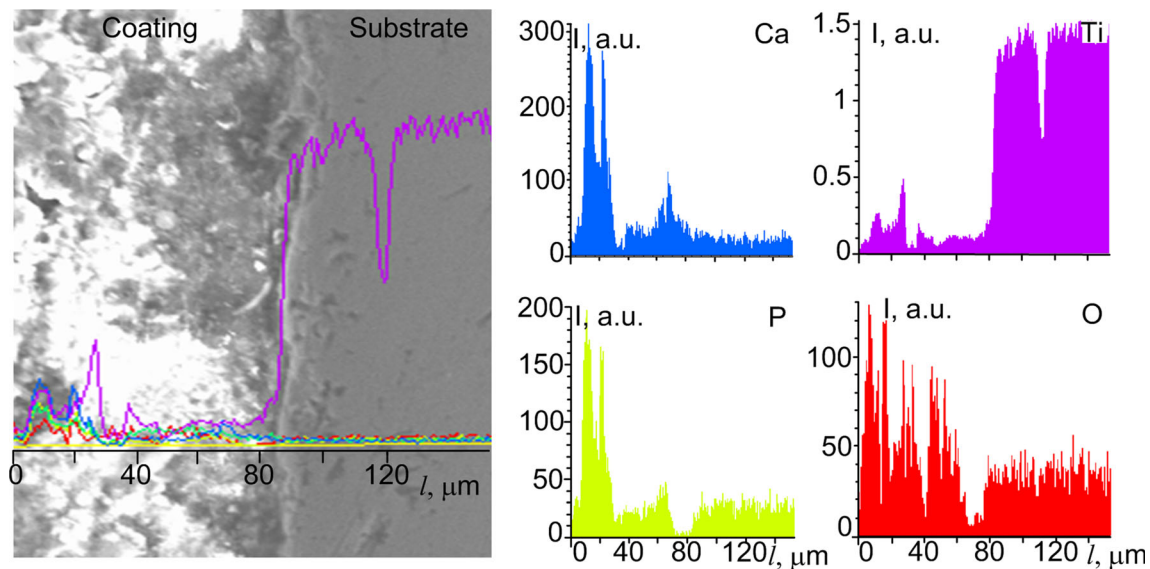


Fig. 6 SEM cross-sectional image of the MAO specimen prepared at 140 V for 2 min, and EDS depth profiles of calcium, titanium, phosphorus and oxygen

OCP from the beginning of the exposure to 350 s demonstrates a typical for these tests oscillation potential, possibly indicating an active-passive behavior caused by local oxidation. Then, an increase in the OCP to -0.054 V is observed, followed by its stabilization. Such potential changes are characteristic for the surface passivation. The OCP for the coating formed at 160 V is positively shifted by 0.03 V (Fig. 7, curve 2), leading to a low thermodynamic tendency toward corrosion. It should be noted that in the time range of 0...455 s, there is a sharp increase in the OCP to -0.020 V followed by its decrease (Table 1). The curve representing the coating deposited at a

voltage of 180 V shifts to more negative values by 0.043 V (Fig. 7, curve 3). An initial drop of the OCP value is soon followed by subsequent recovery. By increasing deposition time from 1 to 2 min at the applied voltage of 140 V, the OCP shifts in a positive direction by 0.073 V (Fig. 7, curve 4) that indicates higher resistance of the HA coating to corrosion.

Figure 8 presents the potentiodynamic polarization data for CP-Ti with HA coatings in Ringer's solution at a temperature of 37 °C. The anodic branches of all polarization curves show two passivation regions that are located at different potentials depending on the HA composition. It should be noted that the

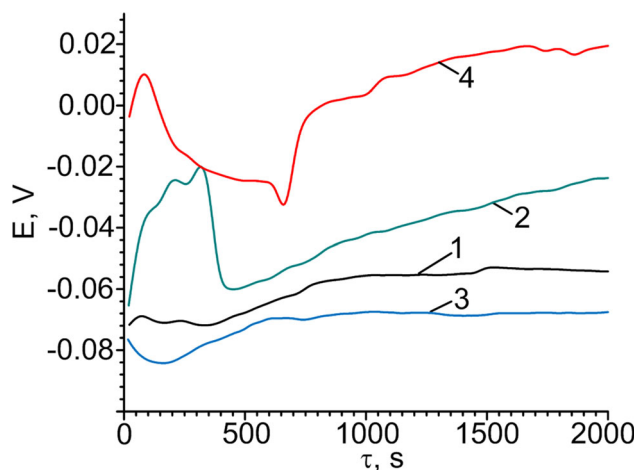


Fig. 7 Open-circuit potential vs. time curves for hydroxyapatite coatings in Ringer's solution at 37 °C: deposition time of 1 min: 1-140 V, 2-160 V, 3-180 V; deposition time of 2 min: 4-140 V

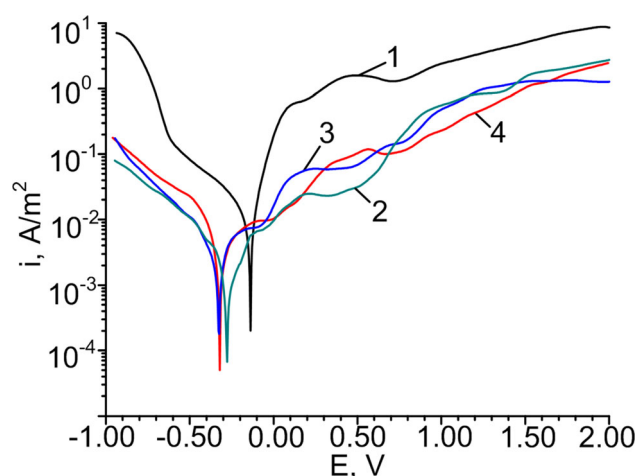


Fig. 8 Potentiodynamic polarization curves for hydroxyapatite coatings in Ringer's solution at 37 °C: deposition time of 1 min: 1-140 V, 2-160 V, 3-180 V; deposition time of 2 min: 4-140 V

corrosion potentials determined from the potentiodynamic polarization curves are lower compared to those obtained from the OCP measurements (Table 1).

For the HA coating prepared at the applied voltage of 140 V (Fig. 8, curve 1), the first passivation region is observed at the potential range from -0.122 to 0.230 V, and the passivation current density is 0.64 A/m². The second passivation region is fixed at the potentials of 0.45...0.72 V, and the passivation current density is 1.5 A/m².

The highest corrosion current density (Table 1) was observed for the HA coating formed at 140 V due to formation of defects (cracks) on its surface during MAO (Fig. 9a) that accelerates the dissolution of hydroxyapatite surface. Anawati

Table 1 Corrosion parameters of CP-Ti with HA coatings in Ringer's solution at 37 °C

U, V/τ, min	OCP, V	E_{corr} , V	i_{corr} , A/m ²
140/1	-0.054	-0.137	0.0084
160/1	-0.024	-0.268	0.0017
180/1	-0.067	-0.345	0.0020
140/2	0.019	-0.309	0.0028

et al. (Ref 22) investigated that samples with more defects increase the anodic current density thereby deteriorating protective properties of the HA coating. According to the EDS analysis, the Ca/P ratio after corrosion increases from 1.54 to 1.65 compared. Perhaps, it is due to the completion of the hydroxyapatite that was observed by S. Durdu et al. (Ref 16): the surface of the MAO coating was covered with the newly formed layer of hydroxyapatite in SBF.

By increasing applied voltage to 160 V (Fig. 8, curve 2), the anodic current for the HA coating decreases by 1-2 orders of magnitude and the corrosion current density—by five times (Table 1). At the potentials of -0.126...-0.041 V, the first passivation region is observed (the passivation current density being ~ 0.006 A/m²). The second passivation region is observed in the potential range from 0.185 to 0.370 V, and the passivation current density is 0.023 A/m². Lower passivation currents may indicate that the HA coating prepared at 160 V is more resistant to corrosion than the coating deposited at 140 V due to more homogeneous surface layer that can block dissolution processes. It is observed a local dissolution of the surface layer (Fig. 9b), which is confirmed by the EDS analysis that shows a decrease in the content of elements after corrosion: O (65.47 at.% versus 70.59 at.%), Ti (8.84 at.% versus 9.92 at.%), Ca (12.97 at.% versus 13.9 at.%), P at.% (7.86 at.% versus 8.22 at.%). The corrosion products are fixed on the surface (Fig. 9b).

By increasing applied voltage during MAO to 180 V, the anodic current increases by 3 times and corrosion current density by 1.2 times (Fig. 8, curve 3), obviously, due to the increase in the porosity of the coating (Ref 25). At potentials from -0.155 to -0.064 V, the first passivation region is observed (the passivation current density is ~ 0.007 A/m²). The second passivation region is fixed in the potential range from 0.18 to 0.41 V (the passivation current density is 0.059 A/m²). According to the SEM analysis, the dissolution is observed over the entire surface of hydroxyapatite coating (Fig. 9c). It is confirmed by EDS analysis because the decrease in the content of elements after corrosion was recorded: Ca (11.65 at.% versus 13.04 at.%), P (7.58 at.% versus 8.28 at. %). The content of oxygen on the surface increases from 68.60 to 69.18 at.% due to the formation of corrosion products such as titanium oxides (Ref 4).

The course of the anodic curve for CP-Ti with HA coating formed at 140 V for 1 and 2 min is similar (Fig. 8, curves 1, 4), but the anodic dissolution of surface at higher deposition time

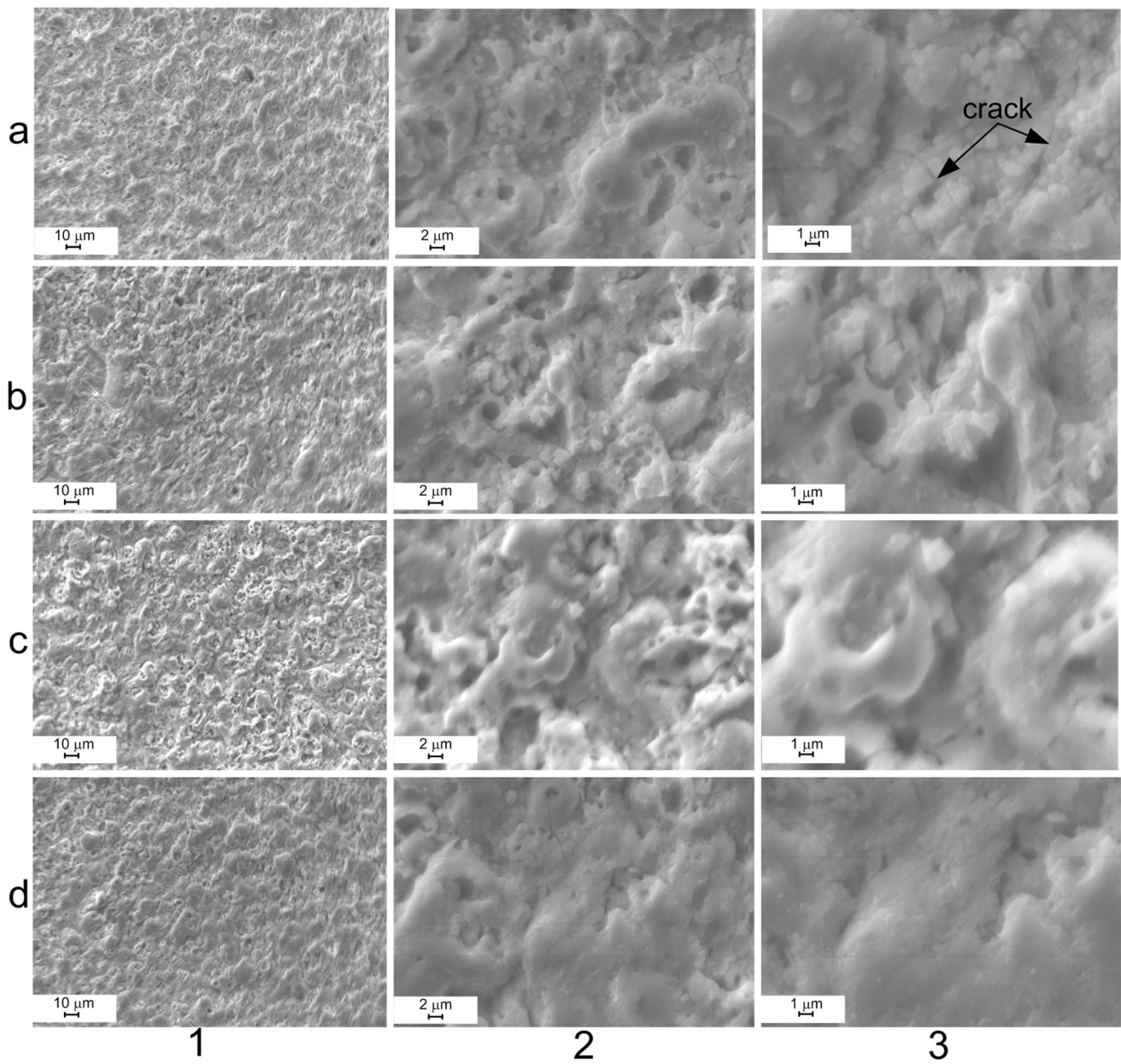


Fig. 9 SEM images of corroded CP-Ti with hydroxyapatite coatings formed after 1 min of MAO: 140 V (a); 160 V (b); 180 V (c); 2 min: 140 V (d); 1 ($\times 1000$), 2 ($\times 5000$) and 3 ($\times 10,000$) magnification images are presented at the left, middle and right columns, respectively

occurred at currents that are from 1 to 2 orders of magnitude larger. The corrosion current density is reduced by 3 times that indicates higher corrosion resistance of the HA coating deposited at longer deposition time.

If we consider the potential range from 400 to 500 mV (Fig. 10) defined by Velten et al. (Ref 27) as the potential of the human body, the passive current density of MAO-surface

coating deposited at 160 V is the lowest, which contributes to the best corrosion resistance.

The electrochemical impedance spectroscopy (EIS) was also used to better investigate the corrosion behavior of the MAO coatings produced at different applied voltages and times as presented in form of Nyquist plot (Fig. 11). Figure 12 is a proposed equivalent circuit which had an acceptable fitness

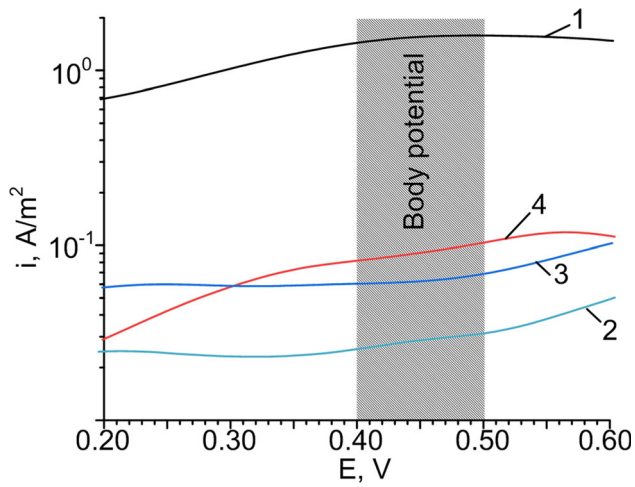


Fig. 10 Zoom of potentiodynamic polarization curves in the potential range from 0.2 V to 0.6 V for hydroxyapatite coatings in the Ringer's solution at 37 °C: deposition time of 1 min: 1-140 V; 2-160 V; 3-180; deposition time of 2 min: 4-140 V

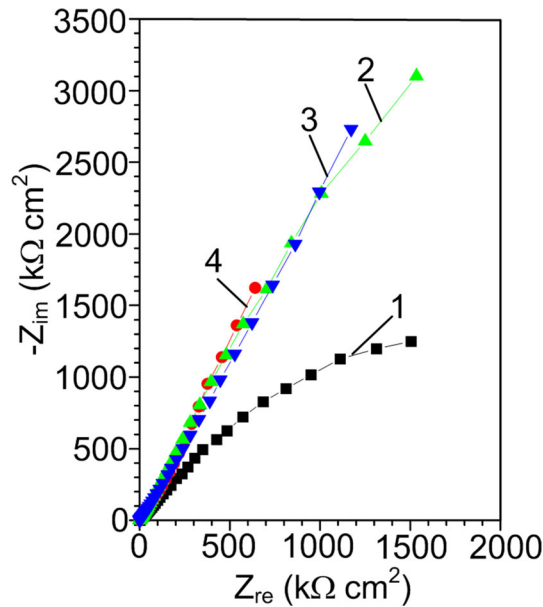


Fig. 11 Nyquist plots for hydroxyapatite coatings in Ringer's solution at 37 °C: deposition time of 1 min: 1-140 V, 2-160 V, 3-180 V; deposition time of 2 min: 4-140 V

with the data obtained from EIS for the coated samples. The equivalent circuit has two time constants that correspond to the coating with an outer porous layer that was formed due to the plasma interaction between the substrate and electrolyte and the barrier layer that was formed due to the applied voltage over the metal (Ref 28). The HA layer and the CaHPO_4 , CaTiO_3 layers can be considered in fact as one unique uniform porous layer from the electrochemical point of view, due to the fact that the

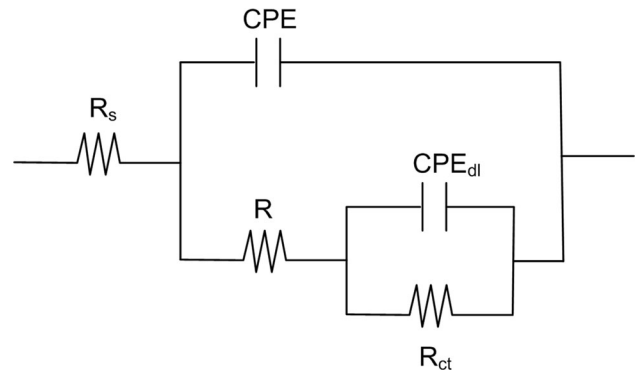


Fig. 12 Equivalent electric circuit fitted to the electrochemical impedance spectroscopy data

HA layer was not compact and filled the pores that characterize the MAO coating.

The calculated equivalent circuit elements are shown in Table 2. The resistance of the outer porous layer (R) is smaller than that of the inner compact layer (R_{ct}) in all samples. According to the results listed in Table 2 and EIS plots shown in Fig. 11, the corrosion resistance of samples ($R + R_{ct}$) increased by increasing the applied voltage from 140 to 160 V and decreased to 180 V, the sample coated in 160 V had the highest overall resistance. The thickness of the coating and higher HA formation increased by increasing the voltage 140 to 160 V which caused higher corrosion resistance. This may be due to the coverage of HA on the titanium at 160 V that prevented the aggressive ions from easily moving into the pores. Consequently, the resistance of porous layer strongly increased. The results from EIS were consistent with the polarization results which confirm that the best corrosion behavior was achieved after 160 V of MAO coating.

The effect of the deposition time on corrosion behavior was also studied by the EIS plots shown in Fig. 11 and the data listed in Table 2. The resistance of both inner layer (R_{ct}) and outer layer (R) increased when the processing time extended to 2 min due to an increase in the thickness of coatings. In addition, higher HA formation for longer times was contributed to an increase in the resistance of porous outer layer.

4. Conclusions

The porous calcium phosphate coatings with a spherical structure were deposited on CP-Ti by the MAO technique in an alkaline electrolyte (hydroxyapatite + 1 M potassium hydroxide) at applied voltage of 140, 160, 180 V and deposition time of 1 and 2 min. It was determined that under such conditions the MAO coatings contain phases of calcium titanate CaTiO_3 , dicalcium phosphate anhydrous (monetite) CaHPO_4 and hydroxyapatite $\text{Ca}_{10}(\text{PO}_4)_6(\text{OH})_2$. It was determined that by increasing applied voltage from 140 to 160 V the Ca/P ratio increases from 1.54 to 1.69, i.e., the composition of HA

Table 2 Parameters of specific elements of equivalent circuits fitted to electrochemical impedance spectra

U, V/ τ , min	$R_s, \Omega \cdot \text{cm}^2$	$R, \Omega \cdot \text{cm}^2$	$R_{ct}, \text{k}\Omega \cdot \text{cm}^2$	CPE _{dl} , F·Hz ¹⁻ⁿ		CPE F·Hz ¹⁻ⁿ	
				Y_{dl}	n_{dl}	Y	n
140/1	26,476	17,266	180.8	8.6494×10^{-6}	0.75	3.1135×10^{-6}	0.73
160/1	94,373	67,460	363.2	1.7540×10^{-10}	0.75	8.2251×10^{-6}	0.72
180/1	86,730	42,617	301.4	5.1650×10^{-5}	0.64	7.6849×10^{-6}	0.76
140/2	28,475	23,610	286.8	5.1650×10^{-10}	0.68	4.3142×10^{-6}	0.67

approaches to biological one. It was shown that increasing deposition time from 1 to 2 min at voltage of 140 V promotes the growth of hydroxyapatite phase with Ca/P = 1.64. It was determined that by increasing Ca/P ratio the corrosion resistance of CP-Ti with HA coatings in Ringer's solution at a temperature of 37 °C is improved. The best corrosion protection is provided by the coating deposited at 160 V, 1 min, when the thickness of the coating and HA formation are the highest.

References

- J.M. Ríos, D. Quintero, J.G. Castaño, F. Echeverría, and M.A. Gómez, Comparison Among the Lubricated and Unlubricated Tribological Behavior of Coatings Obtained by MAO on the Ti₆Al₄V Alloy in Alkaline Solutions, *Tribol. Int.*, 2018, **128**, p 1–8. <https://doi.org/10.1016/j.triboint.2018.07.010>
- J.M. Hernández-López, A. Conde, J.J. de Damborenea, and M.A. Arenas, Electrochemical Response of TiO₂ Anodic Layers Fabricated on Ti₆Al₄V Alloy with Nanoporous, Dual and Nanotubular Morphology, *Corros. Sci.*, 2016, **112**, p 194–203. <https://doi.org/10.1016/j.corsci.2016.07.021>
- P. Xiu, Z. Jia, J. Lv, C. Yin, H. Cai, C. Song, and Y. Cheng, Hierarchical Micropore/Nanorod Apatite Hybrids in-situ Grown from 3-D Printed Macroporous Ti₆Al₄V Implants with Improved Bioactivity and Osseointegration, *J. Mater. Sci. Technol.*, 2017, **33**, p 179–186. <https://doi.org/10.1016/j.jmst.2016.05.013>
- E. Urbańczyk, A. Krzakała, A. Kazek-Kęsik, J. Michalska, A. Stolarczyk, G. Dercz, and W. Simka, Electrochemical Modification of Ti-13Nb-13Zr Alloy Surface in Phosphate Based Solutions, *Surf. Coat. Technol.*, 2016, **291**, p 79–88. <https://doi.org/10.1016/j.surfcoat.2016.02.025>
- E. Ahounbar, S. Mohammad, M. Khoei, and H. Omidvar, Characteristics of in-situ Synthesized Hydroxyapatite on TiO₂ Ceramic via Plasma Electrolytic Oxidation, *Ceram. Int.*, 2019, **45**, p 2909–4146. <https://doi.org/10.1016/j.ceramint.2018.10.206>
- C.A. Antônio, N.C. Cruz, E.C. Rangel, R.C.C. de Rangel, T.E.S. do Araujo, S.F. Durrant, B.A. Más, and E.A.R. Duek, Hydroxyapatite Coating Deposited on Grade 4 Titanium by Plasma Electrolytic Oxidation, *Mater. Res.*, 2014, **17**, p 1427–1433. <https://doi.org/10.1590/1516-1439.286914>
- S. Lederer, S. Sankaran, T. Smith, and W. Fürbeth, Formation of Bioactive Hydroxyapatite-Containing Titania Coatings on CP-Ti₄+ Alloy Generated by Plasma Electrolytic Oxidation, *Surf. Coat. Technol.*, 2019, **363**, p 66–74. <https://doi.org/10.1016/j.surfcoat.2019.02.030>
- H.-J. Song, M.-G. Kim, W.-J. Moon, and Y.-J. Park, Formation of Hydroxyapatite Nanorods and Anatase TiO₂ on CaTiO₃ Powder using Hydrothermal Treatment, *Mater. Sci. Eng. C*, 2011, **31**, p 558–561. <https://doi.org/10.1016/j.msec.2010.11.024>
- S. Durdu, M. Usta, and A.S. Berkem, Bioactive Coatings on Ti₆Al₄V Alloy Formed by Plasma Electrolytic Oxidation, *Surf. Coat. Technol.*, 2016, **301**, p 85–93. <https://doi.org/10.1016/j.surfcoat.2015.07.053>
- J.-Z. Chen, Y.-L. Shi, L. Wang, F.-Y. Yan, and F.-Q. Zhang, Preparation and Properties of Hydroxyapatite-Containing Titania Coating by Micro-Arc Oxidation, *Mater. Lett.*, 2006, **60**, p 2538–2543. <https://doi.org/10.1016/j.matlet.2006.01.035>
- A. Kazek-Kęsik, G. Dercz, I. Kalemba, K. Suchanek, A.I. Kukhareno, D.M. Korotin, J. Michalska, A. Krzakała, J. Piotrowski, E.Z. Kurmaev, S.O. Cholakh, and W. Simka, Surface Characterisation of Ti-15Mo Alloy Modified by a MAO Process in Various Suspensions, *Mater. Sci. Eng. C*, 2014, **39**, p 259–272. <https://doi.org/10.1016/j.msec.2014.03.008>
- M. Montazeri, C. Dehghanian, M. Shokouhfar, and A. Baradaran, Investigation of the Voltage and Time Effects on the Formation of Hydroxyapatite-Containing Titania Prepared by Plasma Electrolytic Oxidation on Ti-6Al-4V Alloy and its Corrosion Behavior, *Appl. Surf. Sci.*, 2011, **257**, p 7268–7275. <https://doi.org/10.1016/j.apsusc.2011.03.103>
- M.-A. Faghihi-Sani, A. Arbabi, and A. Mehdinezhad-Roshan, Crystallization of Hydroxyapatite during Hydrothermal Treatment on Amorphous Calcium Phosphate Layer Coated by MAO Technique, *Ceram. Int.*, 2013, **39**, p 1793–1798. <https://doi.org/10.1016/j.ceramint.2012.08.026>
- J.-H. Ni, Y.-L. Shi, F.-Y. Yan, J.-Z. Chen, and L. Wang, Preparation of Hydroxyapatite-Containing Titania Coating on Titanium Substrate by Micro-Arc Oxidation, *Mater. Res. Bull.*, 2008, **43**, p 45–53. <https://doi.org/10.1016/j.ceramint.2012.08.026>
- A.R. Rafieerad, M.R. Ashra, R. Mahmoodian, and A.R. Bushroa, Surface Characterization and Corrosion Behavior of Calcium Phosphate-Base Composite Layer on Titanium and its Alloys via Plasma Electrolytic Oxidation: A Review Paper, *Mater. Sci. Eng. C*, 2015, **57**, p 397–413. <https://doi.org/10.1016/j.msec.2015.07.058>
- S. Durdu, Ö.F. Deniz, I. Kutbay, and M. Usta, Characterization and Formation of Hydroxyapatite on Ti₆Al₄V Coated by Plasmaelectrolytic Oxidation, *J. Alloys Compd.*, 2013, **551**, p 422–429. <https://doi.org/10.1016/j.jallcom.2012.11.024>
- S.A. Adeleke, S. Ramesh, A.R. Bushroa, Y.C. Ching, I. Sopyan, M.A. Maleque, S. Krishnasamy, H. Chandran, H. Misran, and U. Sutharsini, The Properties of Hydroxyapatite Ceramic Coatings Produced by Plasma Electrolytic Oxidation, *Ceram. Int.*, 2018, **44**, p 1802–1811. <https://doi.org/10.1016/j.ceramint.2017.10.114>
- M. Shokouhfar, C. Dehghanian, and A. Baradaran, Preparation of Ceramic Coating on Ti Substrate by Plasma Electrolytic Oxidation in Different Electrolytes and Evaluation of its Corrosion Resistance, *Appl. Surf. Sci.*, 2011, **257**, p 2617–2624. <https://doi.org/10.1016/j.apsusc.2011.10.064>
- M. Shokouhfar, C. Dehghanian, M. Montazeri, and A. Baradaran, Preparation of Ceramic Coating on Ti Substrate by Plasma Electrolytic Oxidation in Different Electrolytes and Evaluation of its Corrosion Resistance: Part II, *Appl. Surf. Sci.*, 2012, **258**, p 2416–2423. <https://doi.org/10.1016/j.apsusc.2011.10.064>
- M. Okido, K. Kuroda, M. Ishikawa, R. Ichino, and O. Takai, Hydroxyapatite Coating on Titanium by Means of Thermal Substrate Method in Aqueous Solutions, *Solid State Ion.*, 2002, **151**, p 47–52. [https://doi.org/10.1016/S0167-2738\(02\)00603-3](https://doi.org/10.1016/S0167-2738(02)00603-3)
- S. Luo, Q. Wang, and R. Yeb, Chidambaram Seshadri Ramachandran, Effects of Electrolyte Concentration on the Microstructure and Properties of Plasma Electrolytic Oxidation Coatings on Ti-6Al-4V Alloy, *Surf. Coat. Technol.*, 2019, **375**, p 864–876. <https://doi.org/10.1016/j.surfcoat.2019.07.053>
- H. Anawati, H. Tanigawa, T. Asoh, M. Ohno, and S. Kubota, Ono, Electrochemical Corrosion and Bioactivity of Titanium-Hydroxyapatite Composites Prepared by Spark Plasma Sintering, *Corros. Sci.*, 2013, **70**, p 212–220. <https://doi.org/10.1016/j.corsci.2013.01.032>
- E.-J. Kim, Y.-H. Jeong, H.-C. Choe, and W.A. Brantley, Electrochemical Behavior of Hydroxyapatite/TiN Multi-layer Coatings on Ti

- Alloys, *Thin Solid Films*, 2014, **572**, p 113–118. <https://doi.org/10.1016/j.tsf.2014.08.035>
24. L. Benea, E. Mardare, M. Mardare, and J.-P. Celis, Preparation of Titanium Oxide and Hydroxyapatite on Ti-6Al-4V Alloy Surface and Electrochemical Behaviour in Bio-simulated Fluid Solution, *Corros. Sci.*, 2014, **80**, p 331–338. <https://doi.org/10.1016/j.corsci.2013.11.059>
25. M. Kazemi, S. Ahangarani, M. Esmailian, and A. Shanaghi, Investigation on the Corrosion Behavior and Biocompatibility of Ti-6Al-4V Implant Coated with HA/TiN Dual Layer for Medical Applications, *Surf. Coat. Technol.*, 2020, **397**, p 126044. <https://doi.org/10.1016/j.surfcoat.2020.126044>
26. I.M. Pohrelyuk, R.V. Proskurnyak, O.V. Tkachuk, and A. Goral, Influence of the Parameters of Plasma-electrolytic Oxidation on the Formation of Calcium-phosphate Coatings on Titanium, *Mater. Sci.*, 2019, **54**, p 789–795. <https://doi.org/10.1007/s11003-019-00265-4>
27. D. Velten, V. Biehl, F. Aubertin, B. Valeske, W. Possart, and J. Brems, Preparation of TiO₂ Layers on CP-Ti and Ti₆Al₄V by Thermal and Anodic Oxidation and by Sol-Gel Coating Techniques and their Characterization, *J. Biomed. Mater. Res.*, 2002, **59**, p 18–28. <https://doi.org/10.1002/jbm.1212>
28. L. Kostelac, L. Pezzato, A.G. Settimi, M. Franceschi, C. Gennari, K. Brunelli, C. Rampazzo, and M. Dabala, Investigation of Hydroxyapatite (HAP) Containing Coating on Grade 2 Titanium Alloy Prepared by Plasma Electrolytic Oxidation (PEO) at Low Voltage, *Surf. Interfaces*, 2022, **30**, p 101888. <https://doi.org/10.1016/j.surfint.2022.101888>

Publisher's Note Springer Nature remains neutral with regard to jurisdictional claims in published maps and institutional affiliations.

Springer Nature or its licensor (e.g. a society or other partner) holds exclusive rights to this article under a publishing agreement with the author(s) or other rightsholder(s); author self-archiving of the accepted manuscript version of this article is solely governed by the terms of such publishing agreement and applicable law.